Available online at www.sciencedirect.com
ScienceDirect
Geochimica et Cosmochimica Acta 71 (2007) 1130–1144
Geochimica
www.elsevier.com/locate/gca

Structure and dynamics of the water films confined between edges of pyrophyllite: A first principle study

Sergey V. Churakov *

Paul Scherrer Institute, CH-5232 Villigen PSI, Switzerland

Received 9 October 2006; accepted in revised form 21 November 2006

Abstract

Edge sites of clay minerals play a key role for pH dependent sorption of ions from solutions of electrolytes. Pyrophyllite, $Al_2[Si_4O_{10}](OH)_2$, is an important structural prototype for a variety of 2:1 dioctahedral phyllosilicates but in contrast to the other clays has no permanent structural charge. The structure of thin water films confined between most common edges of *1Tc* pyrophyllite: (0 1 0), (1 1 0) and (1 0 0), was analyzed by means of ab initio molecular dynamic simulations. The system setup allowed for a full flexibility of the interfaces and a proton exchange between the edges of pyrophyllite and water molecules in solution. The structure of hydrated surfaces is compared with the recent predictions of static geometry optimizations for edge-vacuum interfaces. All surfaces studied reveal a strong hydrophilic character of edge similar to the hydrated silica surface and the facets of simple layered hydroxides. Spontaneous proton transfer between different surface sites were observed in molecular dynamics simulations of the (0 1 0) interface. The proton bound to the $\equiv$Si—OH site was found to exchange with the $\equiv$Al—OH group by the mechanism $\equiv Si{-}OH + \equiv Al{-}OH \leftrightarrow \equiv Si{-}O^- + \equiv Al{-}OH_2^+$. The direction of the proton transfer agrees with the scale of relative proton affinities for surface sites obtained from the static calculations. Alternatively, the proton attached to the $\equiv Al{-}OH_2$ site exchanges with the $\equiv$Al—OH group. In both reactions, the protons are transferred through the chains of hydrogen bonds formed between water molecules in the solution and the surface sites. The observed mechanisms might be one of the basic schemes for the surface proton diffusion in compacted clays. Kinetics of the proton transfer at edge sites is limited by the rate of rearrangements of the water molecules near interface.

1. Introduction

The dynamics and the structure of confined water in compacted clays is strongly influenced by the interaction of the liquid with the surfaces of minerals (Bergman and Swenson, 2000). At high degrees of compaction, the diffusive transport of the solvated ions and the solvent molecules in clays is substantially retarded compared to the free electrolyte solution because of the surface complexation of ions and the strong ordering of solvent molecules at the solid–liquid interface (Swenson et al., 2000; Molera and Eriksen, 2002; Van Loon et al., 2003; Malikova et al., 2005). These properties of clays make them suitable materials for geochemical barriers and backfill media in repositories for toxic and radioactive wastes.

The basic structural element of phyllosilicates can be imagined as a hexagonally ordered layer of octahedra sandwiched between two tetrahedral siloxane planes, commonly referred to as a TOT-sheet (Grim, 1968). Various isomorphic substitutions in the octahedral and the tetrahedral layers of clay minerals result in a permanent structural charge of the TOT unit. The excess charge is compensated by counterions in the interlayer, which are predominantly the alkali metals. Water molecules penetrate into clays by splitting the TOT units apart in order to complete the hydration shells of counterions in the interlayer. The process is known as swelling and it is well understood thanks to numerous experimental and theoretical studies (Delville, 1991; Boek et al., 1995a,b; Bridgeman et al., 1996; Karaborni et al., 1996; Kutter et al., 2000; Swenson et al., 2000; Hensen and Smit,

* Fax: +41 56 310 2812.
E-mail address: sergey.churakov@psi.ch

0016-7037/$ - see front matter © 2006 Elsevier Inc. All rights reserved.
doi:10.1016/j.gca.2006.11.026

2002; Arab et al., 2003; Boek and Sprik, 2003; Chatterjee et al., 2004; Tunega et al., 2004; Whitley and Smith, 2004; Wilson et al., 2004; Ferrage et al., 2005; Malikova et al., 2005; Odriozola and Aguilar, 2005). Both theory and experiments confirm that the basal plane of uncharged 2:1 phyllosilicates has a slight hydrophobic character (Schader and Yariv, 1990; Warne et al., 2000; Tunega et al., 2002; Arab et al., 2003; Churakov, 2006). Heterovalent substitutions in tetrahedral and octahedral sites of the TOT sheet play the key role for absorption of ions in the interlayer (Delville, 1991; Chatterjee et al., 2000; Sutton and Sposito, 2001; Malikova et al., 2004).

In contrast to the chemically inert basal plane, edges of clay particles are extremely reactive (Bickmore et al., 2003; Churakov, 2006). Experimental studies of crystal growth kinetics have shown that the dissolution/precipitation processes take place predominantly on the edge sites of TOT sheets (Bickmore et al., 2001). The properties of broken clay surfaces are similar to that of the edges and act as strong docking sites for organic molecules (Aquino et al., 2003). At different pH, the structure, the composition and the surface charge of the edge sites change due to proton exchange and adsorption of ions from the solution. In particular, at pH below the point of zero charge the edge sites are positively charged which enables a strong attractive interaction with the negatively charged basal plane of the TOT sheets. Such interaction was found to be critical for the ordering of colloidal aggregates of clay particles (Chang and Sposito, 1996; Kutter et al., 2000). Several types of reactive sites (≡Si—OH, ≡Al—OH, ≡Al—OH_2, ≡Al—O—Si≡) are exposed on the edges of di-octahedral clays (Bickmore et al., 2003; Churakov, 2006). The ≡Si—OH groups are structurally similar to those on the surface of amorphous silica (Warne et al., 2000; Masini and Bernasconi, 2001). The amphoteric ≡Al—OH and ≡Al—OH_2 sites inherit the properties of simple layered hydroxides (Churakov et al., 2004; Wang et al., 2004) or the octahedral surface of kaolinite (Warne et al., 2000; Tunega et al., 2004). The ≡Al—O—Si≡ sites are common in zeolites (Chatterjee et al., 1999).

Structural and dynamic properties of water confined between basal planes of clays have been extensively studied by means of molecular dynamics (MD) and Monte-Carlo simulations (Boek et al., 1995a,b; Chang et al., 1995; Chang et al., 1997; Chang et al., 1998; Malikova et al., 2004). Most of these studies were performed with the classical force fields that do not allow for proton exchange reactions and treat the surface statically constrained under the experimental geometries that neglect important effects of the surface polarization. The lateral facets of the clay minerals were disregarded by previous studies because of inability of the classical force fields to adequately reproduce the complex structure of the edge sites. In the current work, the structure of the bulk water confined between most common edge-facets of pyrophyllite, has been studied using ab initio molecular dynamic simulations for the first time. In contrast to the previous calculations, the method enables for a full flexibility of the interface, polarization effects and a proton exchange between the surface and the solution. The surface geometries are compared to the recent results obtained from the static surface optimizations in vacuum (Churakov, 2006).

Although the composition and structure of the edges in phyllosilicates can be affected by heterovalent substitutions, the uncharged edges of pyrophyllite are the basic model system for a large variety of clays. In the thermodynamic description of the sorption processes the standard binding enthalpies of the protons and ions are referred to the uncharged mineral surfaces (Kallay et al., 2004). The effects of the surface charge due to ion sorption and/or permanent structural charge are considered in the mean field sense as an additional electrostatic potential (Westall and Hohl, 1980). The pyrophyllite can be seen as a standard reference system for the thermodynamic description of sorption on the 2:1 dioctahedral clays. It is used in this work to study the sorption properties of the edge sites not related to the permanent structural charge.

2. Method, simulation setup and uncertainties

Pyrophyllite occurs as triclinic *1Tc* and monoclinic *2M* polytypes which belong to the $C\bar{1}$ and the $C2/c$ space groups, respectively (Lee and Guggenheim, 1981; MacKenzie et al., 1985). Relative displacements of the neighboring TOT-sheets in pyrophyllite result in a wide range of polytypism. The natural samples are usually stacking disordered. Distinct edges of pyrophyllite are characterized by different bond-chain types exposed on the facets. In the disordered samples and the *2M* polytype different bond-chain types occur at the neighboring TOT sheets. In the *1Tc* polytype, only one type of bond-chains occurs at the specified edge. Although the *1Tc* polytype of pyrophyllite is not the most common in nature it is used in this work for computational convenience. The *1Tc* polytype has smaller unit cell size and allows the simulation to have reasonable computational costs. The distinct edge facets of *1Tc* pyrophyllite studied in this work represent all important types of the surface bond-chains known for disordered samples. The effect of stacking disorder on the structure of the edge–water interface is neglected in this work.

Three distinct systems were set up to study the dynamics and the structure of water films confined between the (1 1 0), (0 1 0) and (1 0 0) edges of *1Tc* pyrophyllite, respectively. The total composition of simulation cells corresponds to the formula $Al_8Si_{16}O_{40}(OH)_8 \times 26H_2O$. Among the 26 water molecules, eight are strongly absorbed on the surface, and only 18 effectively belong to the interstitial solution. The size of the supercell in the plane of the interface was constrained by the lattice geometry of pyrophyllite. The dimension of the supercell in the direction normal to the interface was adjusted to retain the specific density of the clay and water at ambient conditions. The starting configuration of the pyrophyllite edge surface was taken from the static calculations (Churakov, 2006).

A fragment of bulk water from classical simulations was taken as an initial configuration of the confined fluid. In order to break the initial configuration of the water film, the confined water was held at 800 K for about 1 ps, while the geometry of the edge and strongly absorbed water remained frozen. Then the systems were slowly cooled to the ambient temperature using simulated annealing technique and equilibrated for at least 5 ps at the target temperature (300 K). The velocity distribution of ionic degree of freedom and fluctuation of Kohn–Sham energies were monitored to ensure equilibration of the system. No systematic trends in energy and velocity distributions were observed. The production runs for more than 10 ps were performed in the microcanonical ensemble. Average temperatures and parameters of simulation cells are summarized in Table 1. The diffusion coefficients of interlayer water were derived from the asymptotic behavior of the mean square displacement.

All the calculations in this work were performed using the density functional theory (Hohenberg and Kohn, 1964; Kohn and Sham, 1965) implemented in the CPMD (1999) simulation package. The exchange and correlation were taken into account by the generalized gradient approximation PBE (Perdew et al., 1996). Interaction of the valence electrons with the core states is described by the pseudopotential formalism. We use the ultrasoft Vanderbilt type pseudopotentials (Vanderbilt, 1990), which allow us to decrease the required basis set dramatically. The wave functions of valence electrons are expanded into the plane wave basis set up to 25 Ry cut-off energy. The ab initio Car-Parrinello MD simulations (Car and Parrinello, 1985) were performed, with a time step of 0.17 fs and a fictitious electron mass of 500 au sampling a single k-point in the centre of Brillouin zone. The accuracy and transferability of the pseudopotentials as well as the convergence of the plane wave basis set expansion were tested against the geometry of small molecules, simple oxides and bulk structure of pyrophyllite. The bond length in the molecules and the lattice parameters of solids could be reproduced within 1% and 2% of the experimental values, respectively. The lattice energy optimization of the bulk pyrophyllite with a four times larger supercell confirmed that the system size is large enough for the convergence with respect to k-points. Additionally a MD simulation of bulk water starting from fully equilibrated Monte-Carlo simulation with SPCE empirical force field was performed to test the ability of the simulation setup to reproduce structural properties of bulk water. The calculated positions of maxima and minima on the oxygen–oxygen radial distribution function (RDF) summarized in Table 2 are in close agreement with the experimental results obtained from neutron scattering (Soper, 2000). The average water coordination number obtained by integration of oxygen–oxygen RDF is also in agreement with the experiment. However, simulated RDFs show higher structuring of water comparing to the experiments (sharper maxima and deeper minima on RDFs). The over-structuring observed in our simulations is in agreement with the previous ab initio studies of bulk water (Grossman et al., 2004; Sit and Marzari, 2005). Possible sources of discrepancies with the experiment are discussed in the following section.

It was noticed recently, that the structural and dynamical parameters of the first principle water obtained by the Car–Parrinello MD are strongly influenced by the simulations setup (Asthagiri et al., 2003; Fernandez-Serra and Artacho, 2004; Grossman et al., 2004; Kuo et al., 2004; Schwegler et al., 2004; VandeVondele et al., 2005). Among the critical parameters that control the outcome of calculations are the exchange-correlation functional, the fictitious electron mass, the system size, and the duration of the equilibration. Systematic testing of different exchange-correlation functionals showed that the BLYP (Becke, 1988; Lee et al., 1988) functional has the best performance for the geometry of water dimers (Sprik et al., 1996). The PBE functional used in this work produces the same results for bulk water as BLYP (Grossman et al., 2004; VandeVondele et al., 2005). Binding energies, geometries

Table 1
Parameters of the supercells, the average temperature and the diffusion coefficient of the centre of mass of confined water for different fluid–solid interfaces

Interface	a [Å] × b [Å] × c [Å]	T [K]	D [m^2 s^{-1}]
(0 1 0)	10.44 × 16.44 × 9.35	306.7	0.27×10^{-9}
(1 1 0)	10.44 × 16.44 × 9.35	295.8	0.28×10^{-9}
(1 0 0)	19.00 × 9.03 × 9.35	298.9	0.35×10^{-9}

Table 2
Parameter of the oxygen–oxygen radial distribution function of water compared with the other ab initio simulations and the experimental data

	R [$g(r)_{max}$] [Å]	$g(r)_{max}$	R [$g(r)_{min}$] [Å]	$g(r)_{min}$
This work[a]	2.71	3.12	3.29	0.42
Sit and Marzari (2005)[b]	2.71	3.21	3.29	0.25
Grossman et al. (2004)[c]	2.71	3.27	3.32	0.46
Kuo et al. (2004)[d]	2.75	3.00	3.30	0.50
Soper (2000)[e]	2.73	2.75	3.36	0.78

[a] Ab initio simulations, 32 PBE-H_2O, 300 K.
[b] Ab initio simulations, 32 PBE-D_2O, 325 K.
[c] Ab initio simulations, 54 PBE-H_2O, 294 K.
[d] Ab initio simulations, 64 BLYP-H_2O, 315 K.
[e] Experimental, neutron diffraction, 298 K.

and vibrational frequencies of PBE-water dimers are also in close agreement with the experiments (Sit and Marzari, 2005). However it is also known that these functionals result in an over-structured RDF for bulk water and in smaller diffusion coefficients (Kuo et al., 2004). The major reason for over-structuring of water in ab initio molecular dynamics simulations is believed to be due to neglecting the proton quantum effects (Grossman et al., 2004; Schwegler et al., 2004; de la Pena and Kusalik, 2006). In principle, the effect of the proton quantum motion can be accounted for with the path integral method (Marx and Parrinello, 1996). To date, such simulations are not possible for a system of reasonable size and time scale. The value of fictitious electron mass used in the calculations was sufficiently small to ensure the adiabatic separation of the electron and nuclear dynamics. The small system size generally leads to a slight over-structuring of the fluid phase or molecular films on solid surfaces (Spohr, 1997a,b; Yeh and Hummer, 2004). Systematic studies have shown the system size effects to be marginal compared to the other computational artifacts (Fernandez-Serra and Artacho, 2004; Kuo et al., 2004). The first ab initio simulations of water, for example, were performed with only 32 molecules, but achieved a remarkable agreement with the experiments (Laasonen et al., 1993). The edge of the supercell in those calculations was equal to 9.6 Å, which is comparable to the lateral dimensions of the interfaces used in our simulations. Analysis of the dynamics of hydrogen bond relaxations in water revealed the existence of two characteristic time scales (Fernandez-Serra and Artacho, 2004). Evolution of the system to the global equilibrium takes place on a very long time scale order of tens to hundreds picoseconds while the local structural characteristics and even the diffusivity seem to equilibrate on a significantly shorter time scale of a few picoseconds. It was demonstrated that the global equilibration of water at ambient condition may require as long as 20 ps simulation run (Fernandez-Serra and Artacho, 2004). Nevertheless, the local relaxations take place on a shorter time scale, order of 2 ps, and we obtain a good description of the local fluid–solid interactions at the interface. It is obvious however that we were not capable of accurately sampling the long period fluctuation during the short simulation time. The longer simulations were not possible due to limitations of the method and available computational resources.

Finally, a methodologically important point related to the density of confined water films should be clarified. The plain wave cutoff used in the simulation is sufficient for accurate prediction of the molecular geometries and relative energies. This basis set, however, is not complete for accurate estimation of the stress tensor (Payne et al., 1992). Additionally the stress is known to converge slowly, so that there is no hope to estimate this property within the given simulation time. Therefore, the pressure was not calculated and the system studied could have been under excess pressure eventually. Insight on the influence of a compression on the structure of confined fluid can be gained from analysis of the behavior of bulk water at high pressures. Both experimental data (Walrafen and Abebe, 1978) and computer simulations (Kalinichev et al., 1999) indicate that the pressure has a minor effect on hydrogen bonding in water at ambient temperature. Despite an insignificant decrease of the intermolecular distances (bonded range) and a little decrease in the hydrogen bond angle the average number of hydrogen bonds per molecule and overall topology of the hydrogen bonding network remain unchanged over the range of pressures studied up to 10 kbar. The response of the water molecules to compression at room temperature is mainly in increasing of a packing of non-bonded nearest neighbors. In this work the structure of the interface is mainly analyzed in terms of intermolecular distances and we are preliminarily interested in the relative interaction of distinct surface groups on the edges with water within a single simulation run. Since the response of the hydrogen bonding network in bulk water was shown to be small we also expect a minor effect of pressure on hydrogen bonding network in confined water. Finally, the relative response of the surface groups within a single simulation is even smaller then the absolute change. Nevertheless, systematic calculations with different densities of the confined fluid are to be done to fully clarify this point.

3. Results and discussion

3.1. Influence of the fluid on the structure of edge sites

Three representative snapshots of the simulation setup for the (010), (100) and (110) interfaces are shown in Fig. 1. The geometries of edges in presence of solution are qualitatively similar to the predictions from the static calculations (Churakov, 2006). The average bond lengths of the surface molecular complexes in the presence of water fluid are compared with the results of the static optimizations of the edge facets exposed to the vacuum in Table 3. For all the studied interfaces the length of the Si—O bonds is almost identical to that predicted by the static calculations. The Al—O contacts in $\equiv Al_2—OH$, $\equiv Al—O—Si\equiv$, $\equiv Al—OH$ and $\equiv Al—OH_2$ are slightly influenced by the presence of the solution. The Al—O bonds in $\equiv Al_2—OH$, $\equiv Al—OH$ and $\equiv Al—O—Si\equiv$ surface sites are elongated by about 2%, while in the $\equiv Al—OH_2$ group the Al—O contacts are shortened. At the same time, the length of OH bonds in $\equiv Al—OH_2$ and $\equiv Si—O^1H$ groups is significantly longer then that in the static calculations. The results can be explained by a different stiffness of the Si—O and Al—O bonds. The stiffer Si—O bonds are hardly affected by the presence of the fluid at the interface. In contrast the relatively soft Al—O contacts in the Si—O—Al bridging bond and, in particular, in $\equiv Al—OH_2$ groups, readily respond to the hydrogen bonding interaction between surface oxygen atoms and water molecules near the interface. Straining of the OH bonds in $\equiv Al—OH_2$ groups due to interaction with the

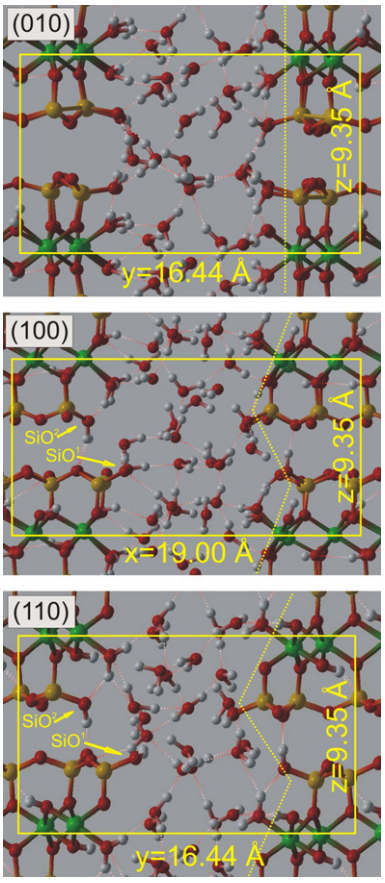

Fig. 1. Snap-shot from MD simulations of the (010), (100) and (110) interfaces. Oxygen atoms are red, aluminum atoms are green, silicon atoms are light-brown and hydrogen atoms are grey. Simulation supercell is marked by a yellow rectangle. "External" (≡Si—O^{1}H) and "internal" (≡Si—O^{2}H) oxygen sites are labeled on (100) and (110) interfaces. Dotted lines schematically trace the extent of solid–fluid interface. Note that (110) and (100) interfaces are not planar.

Table 3
Average bond distances in the surface groups at water–pyrophyllite edge interfaces obtained by MD simulations

	R_{Si-O} [Å]	R_{Al-O} [Å]	R_{OH} [Å]
(010)			
≡SiOH	1.650(1.649)		1.012(0.981)
≡AlOH		1.863(1.833)	0.979(0.974)
≡$AlOH_2$		1.997(2.173)	1.010(0.990)
≡AlOSi≡	1.656(1.658)	1.945(1.910)	
(110)			
≡SiO^{1}H	1.652(1.665)		1.004(0.974)
≡SiO^{2}H	1.650(1.654)		0.986(0.972)
≡Al_2OH		1.912(1.926)	0.980(0.975)
≡$AlOH_2$		1.967(2.068)	1.004(0.987)
≡AlOSi≡	1.606(1.610)	1.846(1.810)	
(100)			
≡SiO^{1}H	1.663(1.668)		1.012(0.976)
≡SiO^{2}H	1.656(1.660)		0.996(0.972)
≡Al_2OH		1.921(1.904)	0.979(0.973)
≡$AlOH_2$		2.036(2.064)	1.014(0.995)
≡AlOSi≡	1.608(1.609)	1.844(1.815)	

Results from the static calculations for the pyrophyllite edge exposed to vacuum are given in brackets for comparison (Churakov, 2006).

molecules in the solution is compensated by pronounced contraction of the Al—O distances.

3.2. Structure of water films near the interface

The running coordination numbers for different oxygen sites with respect to hydrogen atoms of water molecules in solution and surface OH groups on the (010), (110) and (100) edge sites of pyrophyllite are plotted in Fig. 2. The second maximum on the RDF corresponds to the average length of hydrogen bonds (Table 4). The average number of hydrogen bonds (Table 4) is calculated assuming the geometric criterion of hydrogen bonds.(Kalinichev and Churakov, 2001) According to this criterion, two molecules are considered as hydrogen bonded if the distance between oxygen and hydrogen sites is less then 2.4 Å. This threshold corresponds to the position of the second minima on the oxygen–hydrogen RDF of water.

3.2.1. Water-(010) interface

The simulated (010) surface contains four ≡Si—OH groups, two ≡Al—OH sites and two ≡Al—OH_2 complexes on each side of the interface. For every instantaneous configuration, one could distinguish two non equivalent ≡Si—OH sites. One half is situated in the neighborhood of the ≡Al—OH sites, while the other half is located close to the ≡Al—OH_2 groups. As it is shown later the exchange of protons between ≡Al—OH_2 and ≡Al—OH groups introduces a dynamic disorder that results in the equivalence of ≡Si—OH sites if considered as an ensemble average over sufficiently long simulation time.

Oxygen atoms in ≡Si—OH groups accept 1.33 hydrogen bonds in total. The 0.38 hydrogen bonds come from the surface sites. On average, 0.95 water molecules from the interstitial fluid donate hydrogen bonds to ≡Si—OH sites. Hydrogen atoms donate 0.85 hydrogen bonds to the water molecules from the interfacial fluid and 0.14 to the surface oxygen atoms. After about 5 ps of the production run, the proton from the ≡Si—OH group was spontaneously transferred to the ≡Al—OH site, and the bare ≡Si—O^- surface site was formed. Excess negative charge on the ≡Si—O^- complex produces a strong attraction field for the water molecules. The proton free ≡Si—O^- surface site is coordinated by 3.48 hydrogen atoms where only 0.52 are donated by the surface groups and 2.96 are donated by the water molecules from the interstitial fluid. This illustrates that the stabilization of charged surface groups is mainly achieved by the rearrangements of the water molecules at the interface, rather than through the structural changes on the surface and in the bulk of the solid. Although the number of hydrogen bonds from surface sites increased, the main contribution to the coordination is given by the interstitial fluid. A strong reorganization of the water molecules close to ≡Si—O^- sites results in significant structural changes in the neighboring water layers.

Oxygen atoms in the ≡Al—OH groups accept 1.64 hydrogen bonds. The 0.40 hydrogen bonds are accepted

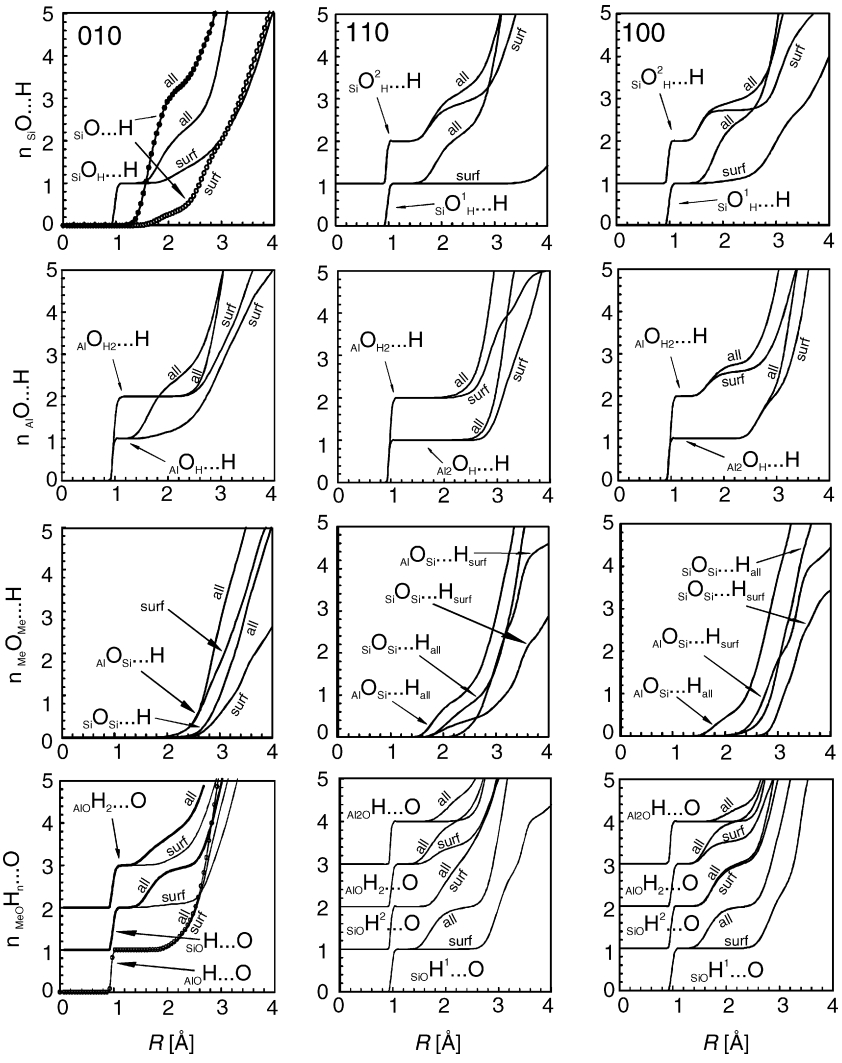

Fig. 2. The running coordination number of the oxygen surface sites with respect to the hydrogen atoms ($n_{\mathrm{SiO}\cdots\mathrm{H}}$, $n_{\mathrm{ALO}\cdots\mathrm{H}}$, $n_{\mathrm{MeOMe}\cdots\mathrm{H}}$) and the coordination number of hydrogen atoms covalently bound to the surface oxygen sites with respect to oxygen atoms in the interstitial water ($n_{\mathrm{MeOH}\cdots\mathrm{O_w}}$). Curves subscribed with "surf" indicate the configuration with respect to hydrogen atoms bonded to surface sites only (water is excluded). The "all" curves consider contributions from both surface sites and water molecules in the solution. The SiO^1 and SiO^2 sites are introduced in Fig. 1. Some curves are shifted along "y" axis to avoid the overlap.

from surface sites and 1.24 bonds are donated by water molecules in the interstitial fluid. The proton of the ≡Al—OH site donates 0.6 hydrogen bonds to the surface oxygen sites and only 0.04 to the interstitial water molecules. The oxygen of the ≡Al—OH_2 site accepts only 0.06 hydrogen bonds. This is explained by configurational difficulties for water molecules to reach the oxygen site since the ≡OH_2 groups are tightly bonded to the surface Al atoms and the OH bonds are pointing towards the interstitial fluid. Each hydrogen atom of the ≡Al—OH_2 groups donates 0.65 hydrogen bonds to the interstitial water molecules and 0.45 to the surface oxygen sites. The ≡Si—O—Si≡ and ≡Si—O—Al≡ sites are spatially separated from the interstitial fluid and do not interact with water.

The strong directional interaction of water molecules with the surface disturbs the common tetrahedral structure of bulk water and introduces a new ordering in the direction normal to the interface. The atomic probability density profile through the clay–water interfaces is given in Fig 3. Based on the positions of minima in the distribution of oxygen sites bonded with two hydrogen atoms, four slices can be distinguished (A, B, C, and D). The distribution is not symmetric relative to the centre of the fluid phase. The asymmetry is caused by several factors. First, as it was addressed in section II, the simulation time is relatively short. Second, the two surfaces were indeed nonequivalent during the production run because of a spontaneous proton transfer between the surface groups. For a sufficiently long expectation time the similar proton transfer events should occur on both sides of the interface. Such a long simulation was not possible due to limited computational resources.

Zone A is represented by the molecules strongly absorbed on the (0 1 0) edge of pyrophyllite. Positions of oxygen atoms in the surface groups are marked by the sharp

Table 4
Total coordination number of hydrogen bonds formed to the surface sites and their average length (maxima of the RDF)

	$n_{\equiv O-Htot}$	$n_{\equiv O\cdots Hsurf}$	$n_{\equiv O\cdots Hw}$	$n_{\equiv H-Otot}$	$n_{\equiv H-Osurf}$	$n_{\equiv H-Ow}$	$\langle R[\equiv O\cdots H]\rangle$ [Å]	$\langle R[\equiv H\cdots O_w]\rangle$ [Å]
(0 1 0)								
Si—OH	2.33	0.38	0.95	1.99	0.14	0.85	1.825	1.65
Si—O	3.48	0.52	2.96					
Al—OH	2.64	0.40	1.24	1.64	0.60	0.04	1.600	
Al—OH_2	2.06	0.04	0.02	2.10	0.45	0.65		1.625
Si—O—Al	0.20	0.20	0.00					
Si—O—Si	0.03	0.02	0.01					
(1 1 0)								
Si—O^1H	2.16	0.00	1.16	1.98	0.00	0.98	1.850	1.725
Si—O^2H	2.17	0.89	0.28	2.22	1.21	0.01	1.775	1.975
Al—OH_2	2.19	0.07	0.12	2.20	0.53	0.67		1.775
Al—(OH)—Al	1.02	0.00	0.02	1.73	0.09	0.64		2.075
Si—O—Al	1.03	0.12	0.91				1.775	
Si—O—Si	0.66	0.36	0.30				2.025	
(1 0 0)								
Si—O^1H	2.52	0.12	1.40	1.99	0.00	0.99	2.825	1.675
Si—O^2H	2.01	0.73	0.28	2.10	1.05	0.05	1.550	1.725
Al—OH_2	2.80	0.60	0.20	2.17	0.68	0.49	1.675	1.625
Al—(OH)—Al	1.04	0.04	0.00	1.44	0.06	0.38		2.075
Si—O—Al	0.88	0.15	0.73				1.775	
Si—O—Si	0.10	0.00	0.10				2.125	

The subscripts surf and *w* indicate that the corresponding atom belongs to a surface group or a water molecule in the fluid. The subscript "tot" indicates the total number of hydrogen bonds formed to the surface site. The last two columns indicate positions of the maxima on the RDF.

maxima on the $O_{(H_2O)}$ and $O_{(OH)}$ distributions. At the distance of −3.5 Å in zone A^I a small maximum in the O-distribution marks the position of the oxygen site in the spontaneously deprotonated ≡Si—OH group. The formation of the ≡Si—O^- surface group is the main factor responsible for the asymmetric distribution of water in the interstitial fluid. The probability density distribution of the angles between the dipole vector of the water molecules and the direction normal to the interface is shown in Fig. 4. Two different conformations are marked by maxima at 12 and 36 degree. A more detailed insight into preferential orientation of water molecules near the interface is obtained from angle distribution of the individual OH vectors of water molecules (Fig. 5). Three maxima at 18, 54 and 90 degrees can be recognized. In the conformation with the smaller angle of dipole vector (12 degrees) both OH bonds of water molecules are pointing outwards from the surface and donate hydrogen bonds to the solution. Each OH vector contributes to the maximum at 54 degrees (Fig. 5). In the conformation with the higher angle (36 degrees), one of the OH bonds is oriented parallel to the surface (maximum at 90 degrees in Fig. 5) while the other one is pointing into the interfacial fluid (the maximum at 18 degrees in Fig. 5). Such geometric interpretation agrees with the statistics of hydrogen bonds (Table 5). The absorbed water molecules donate on average 0.86 hydrogen bonds to the surface and 1.27 hydrogen bonds to the solution. This ratio of hydrogen bonds can be produced by a superposition of two distinct conformations of the strongly bound water molecules. In the first conformation, the dipole moment of the water molecules is orthogonal to the interface, and two OH groups pointing into the solution, this results in the formation of two donating hydrogen bonds to the solution. In the second conformation one OH bond is oriented parallel to the interface and forms a single donating bond to the surface. The second OH vector is pointing to the solution—one donating bond to the surface and one to the water molecules in the solute.

Water molecules in zones B and C are sufficiently close to the interface and can form hydrogen bonds to the surface site. The total number of hydrogen bonds per water molecule in zone B is only slightly greater than in zone C (Table 5). The significant difference is in the fraction of hydrogen bonds formed to surface sites and to the bulk water. Molecules in zone B form up to 70% of hydrogen bonds to the surface and only 30% to the bulk while for the zone C, this ratio is reverse. Angle distributions of dipole moment of water molecules relative to the interface in slices B and C are clearly different (Fig. 4). One can see three distinct maxima in the distribution for zone B. In contrast the distribution in zone C is much more uniform. The difference is emphasized in the angle distribution of individual OH vectors of water molecules (Fig. 5). The distribution for zone B has a sharp maximum at 115 degrees and a flat shoulder between 0 and 85 degrees. This can be interpreted as follows. One OH bond of the water molecule in zone B is oriented almost parallel to the interface (maximum at 115 degree). This OH group forms both donor and acceptor bonds to the surface groups. Another OH vector rotates outward from the interface so that the plane of the molecule changes its orientation from almost parallel to the interface with three hydrogen bonds formed to the surface to almost orthogonal to the interface so that only two hydrogen bonds are formed with the edge.

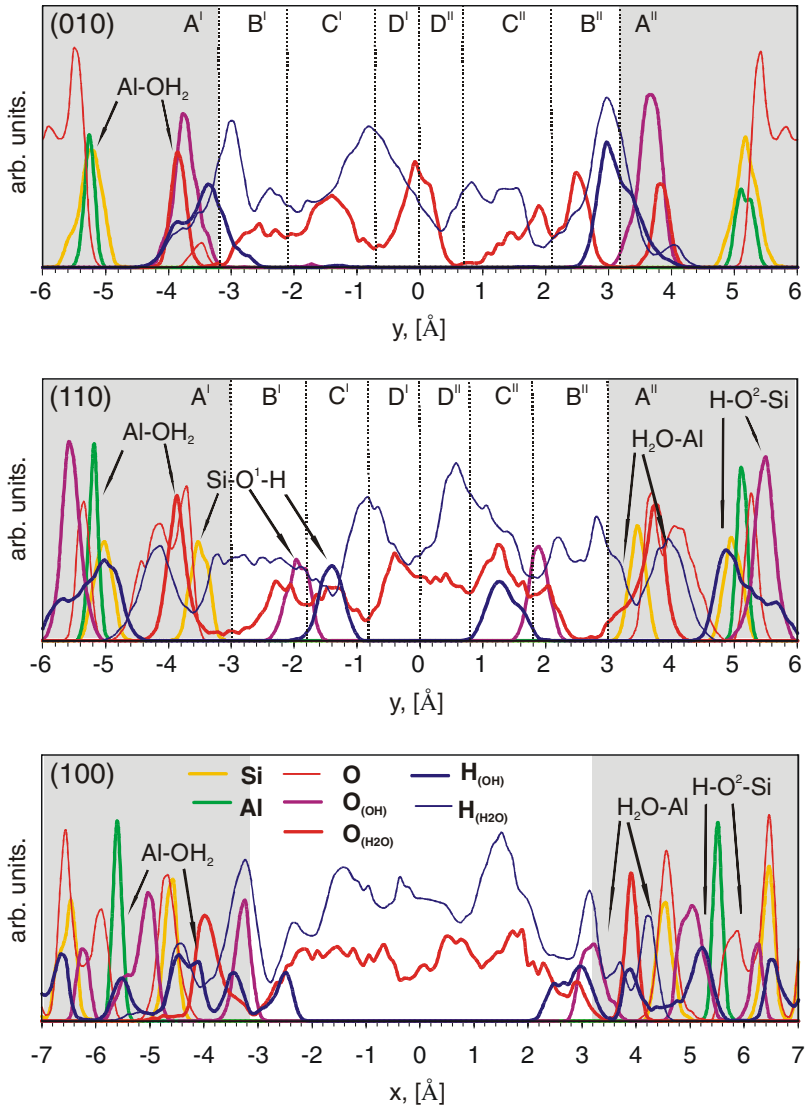

Fig. 3. Atom density profiles through the interstitial fluid and the solid–liquid interfaces. Zero is placed in the middle point of the water film confined by the pyrophyllite edges. "O" denote oxygen atoms not bound to hydrogen atoms, $O_{(OH)}$ are oxygen sites of ≡OH groups. $O_{(H_2O)}$ are central oxygen atoms in $\equiv OH_2$ surface groups and water molecules in the solution. Hydrogen atoms from OH and H_2O groups are denoted by $H_{(OH)}$ and $H_{(H_2O)}$, respectively. The shadowed area schematically indicates the solid phase.

Zone D comprises a central part of the interstitial fluid. Molecules in this group are remote from the interface and do not form hydrogen bonds to the surface. The maximum of $O_{(H_2O)}$ distribution in zone D coincide with the centre of fluid phase. The asymmetric distribution of hydrogen atoms $H_{(H_2O)}$ in slice D suggests that water molecules are preferentially pointing to the "left" interface with the deprotonated $\equiv Si{-}O^-$ site. Compared to other zones, the angle distribution for slice D is the most uniform (Figs. 4 and 5).

3.2.2. Water (110) interface

Two structurally different ≡Si—OH groups on the (110) edge accept the same number of hydrogen bonds (1.16 on the $\equiv Si{-}O^1H$ and 1.17 on $\equiv Si{-}O^2H$ sites, respectively). The internal $\equiv Si{-}O^2H$ sites are hidden from the solution by irregularities of the interface, and make an insignificant contribution to the hydrogen bonding with the water molecules. The 0.89 hydrogen bonds are donated by the surface groups and only 0.28 are accepted from interstitial water. The external $\equiv Si{-}O^1H$ sites are extended into the solution and do not form any hydrogen bonds to the other surface sites. This is compensated by a larger number of hydrogen bonds formed to the interstitial fluid (1.16). Similarly, hydrogen atoms of $\equiv Si{-}O^2H$ sites donate 1.21 bonds to surface oxygen atoms while hydrogen sites from $\equiv Si{-}O^1H$ groups donate 0.98 hydrogen bonds to water molecules. The oxygen site of the $\equiv Al{-}OH_2$ group forms very few acceptor bonds both from surface sites and interlayer water. Every hydrogen atom in the $\equiv Al{-}OH_2$ group donates 0.53 and 0.67 hydrogen bonds to the surface and interstitial water, respectively. The bidentate

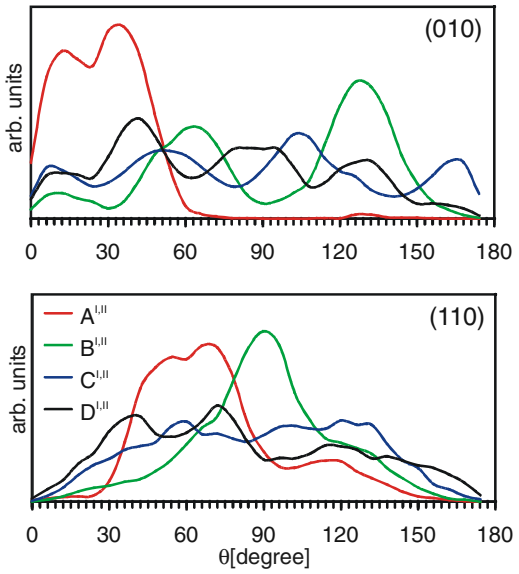

Fig. 4. Angle distribution of the dipole moment of water molecules relative to the "y" direction of the supercell, accumulated separately for molecules located in different zones with respect to the interface (Fig. 3). The distribution is normalized by the total number of molecules in each zone.

≡Al—OH—Al≡ complex is situated far too deep in the structure and, therefore, does not participate in hydrogen bonding with the solution. In contrast to the (0 1 0) interface the bridging oxygen of the ≡Si—O—Al≡ group on the (1 1 0) edge is located much closer to the solution and accepts as many as 0.91 hydrogen bonds from water molecules. Only 0.12 bonds are contributed by the surface sites. The ≡Si—O—Si≡ oxygen is situated deep in the bulk and accepts only 0.36 and 0.30 bonds from the surface sites and the water, respectively.

Due to the specific crystallography of the (1 1 0) edge the fluid-water interface is not planar (see Fig. 1). This fact presents uncertainties in the analysis of the density profile based on the simple distance coordinate. The probability density distribution profile through the fluid–solid interface is shown in Fig. 3. Similar to the (0 1 0) interface four different layers are defined as a function of distance from the centre of the fluid along the "y"-direction of the simulation supercell (Fig. 1). The division is rather fuzzy due to the non-planarity of the interface. The probability density distribution of angles between the dipole moment of water molecules and the "y"-direction of the simulation supercell (Fig. 1) is shown in Fig. 4. The orientational distribution of OH vectors in water molecules and the surface hydroxide groups are shown in Fig. 5.

The average number of hydrogen bonds per water molecule in different zones is given in Table 5. The average number of hydrogen bonds in zone A is different from the statistics for ≡Al—OH_2 groups based on the integration of RDF. The difference originates from the presence of additional water molecules close to the interface. One can recognize these molecules on the probability density distribution in slice A^{II}. The sharp maximum at 3.8 Å in the $O_{(H_2O)}$ distribution (strongly bounded ≡Al—OH_2) forms a shoulder at 3.2 Å. The dipole vector distribution for zone A is dominated by the double hill maximum between 30 and 80 degrees. This maximum is similar to the peak on the distribution for (0 1 0) interface (Fig. 4). The shift to higher angles comparing to the (0 1 0) interface is explained by a bent orientation of the (1 1 0) edge. The orientation of ≡Al—OH_2 groups on (1 1 0) interface can be interpreted in the same way as on the (0 1 0) edge. The broad maximum with the center at 120 degrees is contributed by the water molecules penetrating from the fluid to the open siloxane cavities. These molecules donate hydro-

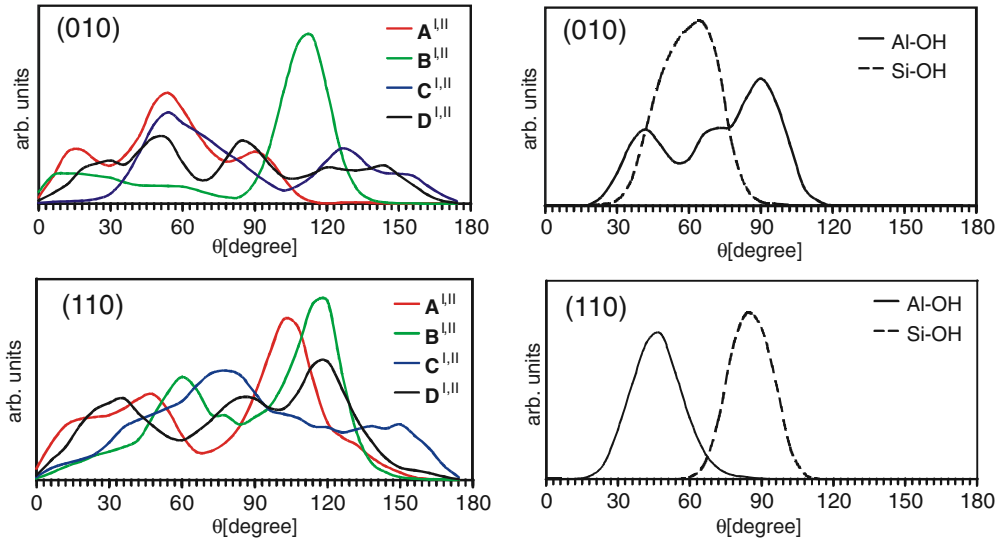

Fig. 5. Probability density distribution of the angles between OH bonds in water molecules, located in different zones relative to the interface (Fig. 3.) and the "y" direction of the supercell pointing outwards from the surface. Separate graphs on the right side show the angle distribution of surface hydroxyl groups bound to Al and Si atoms. Distributions are normalized by the total number of molecules in the corresponding zone.

Table 5
Average number of hydrogen bonds per water molecule in different fluid layers at (0 1 0) and (1 1 0) interfaces ($\langle n_{HB} \rangle$)

Layer	$\langle n_{HB}^{don} \rangle_{surf}$	$\langle n_{HB}^{don} \rangle_{bulk}$	$\langle n_{HB}^{acc} \rangle_{surf}$	$\langle n_{HB}^{acc} \rangle_{bulk}$	$\langle n_{HB}^{don} \rangle$	$\langle n_{HB}^{acc} \rangle$	$\langle n_{HB} \rangle$
(0 1 0)							
A	0.86	1.27	0.05	0.03	2.13	0.07	2.21
B	1.40	0.54	1.32	0.58	1.95	1.91	3.85
C	0.69	1.17	0.67	1.16	1.86	1.83	3.69
D	0.01	1.88	0.00	1.84	1.89	1.84	3.73
(1 1 0)							
A	1.22	0.83	0.56	0.35	2.05	0.90	2.95
B	0.90	0.96	0.81	0.86	1.85	1.67	3.52
C	0.49	1.36	0.42	1.32	1.85	1.74	3.59
D	0.03	1.83	0.07	1.81	1.86	1.88	3.73

Superscripts "don" and "acc" stand for individual contribution of the donor and the acceptor hydrogen bonds. Subscripts "surf" and "bulk" indicate the bonds that are formed to the surface atoms or interstitial water molecules, respectively.

gen bound to ≡Si—O^2H groups and accept protons from ≡Al—OH complexes. In Fig. 5 these molecules contribute to a broad shoulder at 130 degrees. The angle distribution of OH vectors in ≡Si—O^2H and ≡Si—O^1H groups has a single maximum near 90 degrees. In both surface groups, the OH bonds are preferentially elongated orthogonal to the "*y*" axis of the supercell. In contrast to the (0 1 0) interface the angle distribution of ≡Al—OH forms only a single maximum at 48 degree. These groups are deeply located in the solid and have only one type of conformation.

Orientation of water molecules in the zones B and C at (1 1 0) face has certain similarities with the results for (0 1 0) interface. The dipole angle distribution in zone B has a pronounced maximum at 90 degrees with broad shoulders to both sides. The distribution of the individual OH groups has a sharp maximum at 120 degrees and a broad shoulder up to 0 degrees. According to the data in Table 5 the molecules in zone B form equal number of HB to the surface and the bulk fluid. Thus, the molecules in zone B are oriented in such a way that one OH group forms one donating and one accepting bond to the surface. The second OH vector has a broad range of conformations from an inward configuration to an outward pointing orientation relative to the interface. The angular distribution of molecules in zones C and D is substantially uniform and does not allow discriminating different configurations. According to the statistics, molecules in zone C form only about one third of the bonds to the surface sites. Zone D is too far separated from the interface for the HB to be formed with the surface.

3.2.3. Water-(1 0 0) interface

The (1 0 0) interface has two structurally different ≡Si—OH sites. Internal ≡Si—O^2H sites accept 1.01 hydrogen bonds. The 0.73 hydrogen bonds are accepted from the surface groups and only 0.28 are donated by the water molecules. The oxygen site of the ≡Si—O^1H group accepts 1.40 hydrogen bonds from the water molecules and only 0.12 from the surface sites. The ≡Al—OH_2 groups accept 0.6 and 0.2 hydrogen bonds from the surface sites and the water molecules, respectively. Every hydrogen atom of the ≡Al—OH_2 site participates in 0.49 hydrogen bonds to water molecules and 0.68 to surface sites. The bidentate ≡Al—OH—Al≡ group is deeply buried in the bulk and is not involved in the hydrogen bonding. The bridging ≡Si—O—Al≡ oxygen site forms 0.73 bonds to the water and 0.15 to the surface groups. The ≡Si—O—Si≡ site is spatially far away from the interface and therefore does not interact with water.

The probability density distribution near the (1 0 0) interface is shown in Fig. 3. One can recognize strongly bonded water molecules in ≡Al—OH_2 complexes and the surface OH groups. An unambiguous subdivision in the separate water layer is not possible because of a strong irregularity of the interface. This does not mean however that water near the (1 0 0) edge is less structured then near the (0 1 0) and (1 1 0) interfaces. Geometry of the (1 0 0) edge is so complex that structurally different water layers overlap on the selected projection.

3.3. Proton exchange between edges sites

The equilibrium structure of edge sites predicted in static calculations corresponds to the surface geometry with the lowest possible energy at zero Kelvin. At non-zero temperatures, the entropy favors the thermal disorder in the system. At ambient conditions, the average occupation on different oxygen sites by protons should correspond to the equilibrium protonation constants of individual surface sites. The averaging is assumed both over ensemble and time. The atomistic picture of thermodynamic equilibrium implies a dynamic exchange of protons between the solution and the surface, as well as the proton exchange between different sites on the surface. The rate of proton exchange depends on the height of the energy barrier required to break the ≡O—H bond. In most cases, the activation barrier for the proton transfer reaction is too high to observe the proton exchange directly in a short MD simulation. In a special case of strong hydrogen bonding, interaction with the molecules in solution can be sufficient to dramatically reduce the activation barrier for the proton

exchange. In such situation the proton hopping may occur in conventional MD simulations.

In MD simulations of the (0 1 0) interface, a spontaneous proton transfer among ≡Si—OH and ≡Al—OH sites was observed after ~5 ps of the production run which was started after more than 10 ps of equilibration. Snapshots illustrating the mechanism of the proton exchange are shown in Fig. 6. The reaction proceeds in two basic steps. Initially, a water molecule near the surface dissociates, giving a proton to the surface ≡Al—OH group:

$$\equiv Al{-}OH + H_2O_{sol} \rightarrow Al{-}OH_2^+ + OH^-_{sol} \quad (1)$$

The newly formed hydroxyl ion approaches the ≡Si—OH group, and the surface donates a proton back to the fluid:

$$\equiv Si{-}OH + OH^-_{sol} \rightarrow \equiv Si{-}O^- + H_2O_{solv} \quad (2)$$

The sum of these two reaction steps results in proton transfer from ≡Si—OH to ≡Al—OH surface sites:

$$\equiv Al{-}OH + \equiv Si{-}OH \rightarrow \equiv Al{-}OH_2^+ + \equiv Si{-}O^- \quad (3)$$

After a short time (about 0.25 ps) the proton on the $\equiv Al{-}OH_2^+$ group was transferred back to the ≡Si—O⁻ site following the same reaction mechanism and the initial surface configuration was recovered. The presence of aqueous solution near the interface is essential for the success of the reaction and the stability of the reaction products. Molecules in the solution act as a transport medium for the protons. When the proton is successfully transferred, water molecules in the fluid rearrange to screen the charge redistributed on the surface. The average coordination number of ≡Si—OH by hydrogen atoms from the solution is 0.95 (Table 4). After the proton transfer, the ≡Si—O⁻ site is coordinated by 2.96 hydrogen atoms of water molecules (Table 4) with very short hydrogen bonds of about 1.5 Å (see Fig. 2). The proton transfer induces significant rearrangements in the water structure near the deprotonated sites. The efficient screening of charged ≡Si—O⁻ sites makes it possible to stabilize the newly formed meta-stable surface configuration. The presence of solution substantially reduces the energy of reaction products and the activation barrier compared to the same process in gas phase.

Another type of proton exchange was observed between $\equiv Al{-}OH_2$ and ≡Al—OH sites (Fig. 7). The composition of the surface before and after the proton transfer remains unchanged (same surface concentration of $\equiv Al{-}OH_2$ and ≡Al—OH groups). The newly formed configurations differ only by the long-range arrangements of the surface sites. The energy difference of the products and reactants is expected to be small. Essential preconditioning for this type of proton transfer is the formation of a chain of hydrogen bonds connecting the surface sites. The reaction takes place by the mechanism:

$$\equiv Al^{I}{-}OH \cdots H^{I}OH \cdots H^{II}OH \cdots H^{III}HO{-}Al^{II}\equiv \rightarrow \equiv Al^{I}{-}OHH^{I} \cdots OHH^{II} \cdots OHH^{III} \cdots HO{-}Al^{II}\equiv \quad (4)$$

Three protons are transferred simultaneously which eventually results in an exchange of the proton between $\equiv Al^{I}{-}OH$ and $\equiv Al^{II}{-}OH_2$ groups.

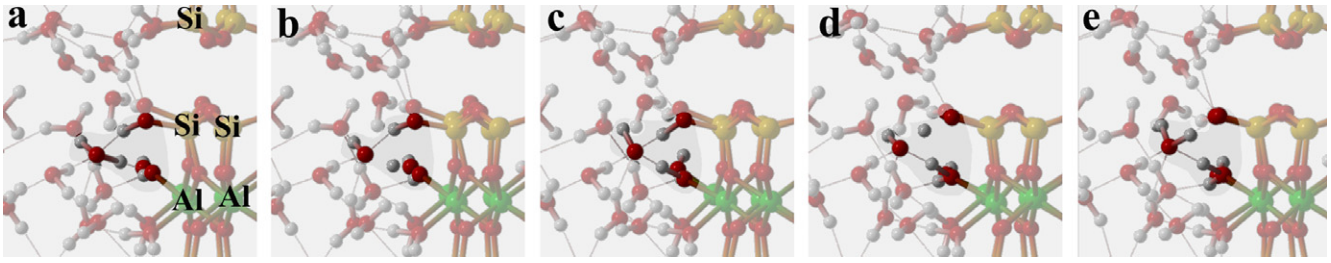

Fig. 6. Example of the proton transfer reaction on the (010) edge of pyrophyllite obtained by first principle molecular dynamics simulations at 300 K. (a) Pyrophyllite surface with ≡Al—OH and ≡Si—OH groups. (b) Dissociation of the water molecule in solution and proton sorption on the ≡Al—OH site. (c) Formation of a solvated OH group and a $\equiv Al{-}OH_2$ surface complex. (d) The ≡Si—OH surface complex donates the proton to the solvated OH group. (e) Finally, the surface consists of the ≡Si—O and $\equiv Al{-}OH_2$ complexes. The color legend is given in Fig. 1.

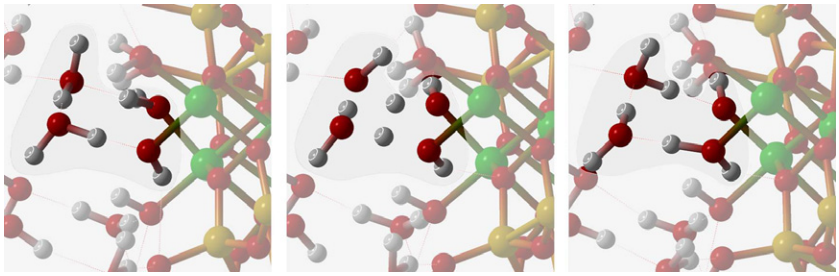

Fig. 7. Proton transfer reaction between $\equiv Al{-}OH_2$ and ≡Al—OH surface groups on the (0 1 0) edge of pyrophyllite. Left and right slides are the initial and final state of the system. The middle slide shows the transition states of the simultaneous transfer of the protons between water molecules in the fluid and two surface groups. The color legend is given in Fig. 1.

Experimental studies of different smectites showed the ion conductivity to have substantial protonic contribution (Poinsignon, 1997; Aliouane et al., 2002). Proton transfer reactions observed in our simulation may be an important component of the ion conductivity in compacted clays. Although the simulation time is not sufficient to derive the proton diffusion coefficients the insight on the mechanism of surface proton diffusion can still be gained from the single proton transfer events. More accurate results on the proton diffusion kinetics could be obtained using with more advanced techniques like thermodynamic integration (Trout and Parrinello, 1999) or metadynamics (Iannuzzi et al., 2003; Churakov et al., 2004). Such simulations are beyond the scope of this study.

One of the basic questions of diffusion kinetics is the nature of the reaction-limiting step. Mechanisms of the proton diffusion in water have been discussed in details (Agmon, 1995). In the bulk water, the kinetics of proton diffusion is limited by the reorganization of solvent molecules. For proton transfer reactions observed in our simulations the structural arrangements of the molecules are an essential part of the reaction mechanism. The proton transfer itself occurs at a significantly shorter time scale. Therefore one can argue that the kinetics of surface diffusion of protons on edges of pyrophyllite is limited by the structural arrangements of solvent molecules at the interface.

3.4. Proton affinity of surface sites and the composition of edges

In the previous work, the composition of edges of pyrophyllite was obtained based on the static optimization of the surface exposed to the vacuum (Churakov, 2006). The proton affinity of sites was estimated using enthalpy of (de)protonation in gas phase, effective charges on oxygen atoms, and the Fukui function formalism. It is important to test whether the predictions of static calculations agree with results of MD simulations for liquid–solid interfaces. The coordination number of oxygen sites and the average length of hydrogen bonds can be considered as an indicator of the proton affinity of surface oxygen sites. Large coordination numbers and short hydrogen bond distances indicate a higher proton affinity of the test site. For weakly bonded protons, the stretching of OH bonds in the solution relative to the gas phase should be stronger. The $\equiv$Al—OH groups on the (0 1 0) edge have higher coordination numbers than $\equiv$Si—OH sites (Table 4). One can also see that the lengthening of the OH groups in the presence of interlayer water is much stronger for $\equiv$Si—OH and $\equiv$Al—OH_2 sites at the (0 1 0) interface than that for $\equiv$Al—OH groups (Table 3). Static calculations predicted $\equiv$Si—OH and $\equiv$Al—OH_2 to be proton donors and the $\equiv$Al—OH sites to act as proton acceptors. This picture is also in agreement with the mechanism of proton transfer reactions observed in the simulations. In both cases, $\equiv$Al—OH sites accepted a proton either from the $\equiv$Si—OH or the $\equiv$Al—OH_2 sites.

Considering $\equiv$Si—O^1H and $\equiv$Si—O^2H sites at the (1 0 0) and (1 1 0) interfaces some discrepancies can be found. According to the static calculations $\equiv$Si—O^1H sites have the higher deprotonation enthalpy than $\equiv$Si—O^2H groups (Churakov, 2006). On the other hand in the presence of solution, the OH bonds on $\equiv$Si—O^1H sites are much more elongated compared to those in vacuum. The $\equiv$Si—O^1H and the $\equiv$Si—O^2H sites on the (1 1 0) interface have the same number of hydrogen bonds. On the (1 0 0) edge $\equiv$Si—O^1H sites have higher coordination numbers than $\equiv$Si—O^2H groups. This would mean that $\equiv$Si—O^1H groups can be deprotonated more easily than $\equiv$Si—O^2H sites in contradiction to the static calculation. The source of these discrepancies might be in the geometrical irregularity of the (1 1 0) and (1 0 0) interfaces. The $\equiv$Si—O^2H groups are located far from the interface and therefore marginally affected by the presence of solution. The $\equiv$Si—O^2H site accepts hydrogen bonds from the surface OH groups so that the effect of solvation is partially included in static calculations. In contrast, $\equiv$Si—O^1H sites form hydrogen bonds exclusively to the molecules in solution. This explains the minor response of the OH groups to the presence of the interlayer solution.

3.5. Comparison with the structure of the bulk water

In order to compare the hydrogen bonding network near edges of pyrophyllite with the bulk fluid a short MD simulation of ab initio water has been performed at ambient conditions with the same exchange-correlation functional and pseudopotentials as for the interface calculations. In bulk water, molecules form on average 3.7 hydrogen bonds (calculated using simple distance criteria). Average length of hydrogen bonds corresponding to the maxima on the OH radial distribution function is 1.8 Å.

The average statistics of hydrogen bonds in different layers of confined water (Table 5) match the value for the bulk fluid. The pronounced difference is observed in the average length of the hydrogen bonds formed to the surface groups (Table 4). The length of hydrogen bonds formed to the surface groups is shorter by 0.1–0.2 Å than in the bulk. The strong hydrogen bonding to the surface undoubtedly indicates a hydrophilic character of the interface.

4. Conclusions

Geometries of the (0 1 0), (1 1 0) and (1 0 0) *1Tc* pyrophyllite–water interfaces obtained by first principle molecular dynamic simulations are in qualitative agreement with the predictions of static structure optimizations of the edge facets exposed to vacuum. The response of the surface to the hydration is manifested by the elongation of surface OH groups by 2–3% and contraction of Al—O bonds. All surfaces studied show a strong hydrophilic character which results in a high degree of ordering of water molecules near the interface. The orientation of molecules at the surface

is similar to that obtained on the idealized surface of hydrated silica (Lee and Rossky, 1994). The OH bonds of water molecules near the interface are oriented parallel to the interface so that at least two hydrogen bonds are formed to the surface.

The simulations give an interesting insight on the mechanism of proton exchange on the hydrated edge sites of the clays. Solution at the interface plays the role of transport medium for the hopping of protons between the surface sites. Kinetics of the proton surface diffusion is limited by the dynamics of the structural rearrangement of the solution molecules near the interface. Water molecules near the interface rearrange to stabilize the products of the proton transfer reactions and lower the activation barrier required for the proton exchange. The directions of the observed proton transfer reactions are in agreement with the relative acidities of the surface sites.

At present, available experimental techniques are not capable of directly probing a given water edge-interface in clay minerals. The thermodynamics studies and AFM spectroscopy confirm the importance of the edges for the stability and the growth of clay particles but does not provide the direct information on the atomistic scale. X-ray absorption spectroscopy, recently applied to study the bulk/vapor water interface and the surface structure of ice (Wilson et al., 2002; Nordlund et al., 2004) is a particularly promising tool for probing the structure of interfaces. Such method focused on the water saturated clays could provide direct evidence for the structural changes in the water–clay interface that can be confronted with the results of the present ab initio simulations. Up to now the simulations remain the only tool to access the structure of the water–clay interface on the atomistic scale.

Acknowledgments

Simulations have been performed on the IBM-SP4 in the CSCS-Manno. The data processing and visualization have been done with the AVS-Express package. The author is grateful to Marcella Iannuzzi and Dmitry Kulik for a fruitful discussion. Special thanks go to Mario Valle for help in visualization of the results. I thank B.R. Bickmore and two anonymous reviewers for fruitful criticism of the manuscript.

Associate editor: James Kubicki

References

Agmon, N., 1995. The Grotthuss mechanism. *Chem. Phys. Lett.* **244**, 456–462.

Aliouane, N., Hammouche, A., De Doncker, R., Telli, L., Boutahala, M., Brahimi, B., 2002. Investigation of hydration and protonic conductivity of H-montmorillonite. *Solid State Ionics* **148**, 103–110.

Aquino, A.J.A., Tunega, D., Haberhauer, G., Gerzabek, M.H., Lischka, H., 2003. Adsorption of organic substances on broken clay surfaces: a quantum chemical study. *J. Comput. Chem.* **24** (15), 1853–1863.

Arab, M., Bougeard, D., Smirnov, K.S., 2003. Structure and dynamics of the interlayer water in an uncharged 2: 1 clay. *Phys. Chem. Chem. Phys.* **5** (20), 4699–4707.

Asthagiri, D., Pratt, L.R., Kress, J.D., 2003. Free energy of liquid water on the basis of quasichemical theory and ab initio molecular dynamics. *Phys. Rev. E* **68**, 041505.

Becke, A.D., 1988. Density-functional exchange-energy approximation with correct asymptotic behavior. *Phys. Rev. A* **38** (6), 3098–3100.

Bergman, R., Swenson, J., 2000. Dynamics of supercooled water in confined geometry. *Nature* **403**, 283–286.

Bickmore, B.R., Bosbach, D., Hochella, M.F., Charlet, L., Rufe, E., 2001. In situ atomic force microscopy study of hectorite and nontronite dissolution: implications for phyllosilicate edge surface structures and dissolution mechanisms. *Am. Mineral.* **86**, 411–423.

Bickmore, B.R., Rosso, K.M., Nagy, K.L., Cygan, R.T., Tadanier, C.J., 2003. Ab initio determination of edge surface structures for dioctahedral 2:1 phyllosilicates: implications for acid-base for reactivity. *Clay. Clay Miner.* **51** (4), 359–371.

Boek, E.S., Coveney, P.V., Skipper, N.T., 1995a. Molecular modeling of clay hydration: a study of hysteresis loops in the swelling curves of sodium montmorillonites. *Langmuir* **11** (12), 4629–4631.

Boek, E.S., Coveney, P.V., Skipper, N.T., 1995b. Monte Carlo molecular modeling studies of hydrated Li-, Na-, and K-Smectites: understanding the role of potassium as a clay swelling inhibitor. *J. Am. Chem. Soc.* **117** (50), 12608–12617.

Boek, E.S., Sprik, M., 2003. Ab initio molecular dynamics study of the hydration of a sodium smectite clay. *J. Phys. Chem. B* **107** (14), 3251–3256.

Bridgeman, C.H., Buckingham, A.D., Skipper, N.T., Payne, M.C., 1996. Ab-initio total energy study of uncharged 2:1 clays and their interaction with water. *Mol. Phys.* **89** (3), 879–889.

Car, R., Parrinello, M., 1985. Unified approach for molecular dynamics and density-functional theory. *Phys. Rev. Lett.* **55** (22), 2471–2474.

Chang, F.R.C., Skipper, N.T., Sposito, G., 1995. Computer-simulation of interlayer molecular-structure in sodium montmorillonite hydrates. *Langmuir* **11** (7), 2734–2741.

Chang, F.R.C., Skipper, N.T., Sposito, G., 1997. Monte Carlo and molecular dynamics simulations of interfacial structure in lithium–montmorillonite hydrates. *Langmuir* **13** (7), 2074–2082.

Chang, F.R.C., Skipper, N.T., Sposito, G., 1998. Monte Carlo and molecular dynamics simulations of electrical double-layer structure in potassium–montmorillonite hydrates. *Langmuir* **14** (5), 1201–1207.

Chang, F.R.C., Sposito, G., 1996. The electrical double layer of a disk-shaped clay mineral particle: effects of electrolyte properties and surface charge density. *J. Colloid Interface Sci.* **178** (2), 555–564.

Chatterjee, A., Ebina, T., Onodera, Y., Mizukami, F., 2004. Effect of exchangeable cation on the swelling property of 2: 1 dioctahedral smectite—a periodic first principle study. *J. Chem. Phys.* **120** (7), 3414–3424.

Chatterjee, A., Iwasaki, T., Ebina, T., 1999. Reactivity index scale for interaction of heteroatomic molecules with zeolite framework. *J. Phys. Chem. A* **103** (15), 2489–2494.

Chatterjee, A., Iwasaki, T., Ebina, T., 2000. A novel method to correlate layer charge and the catalytic activity of 2: 1 dioctahedral smectite clays in terms of binding the interlayer cation surrounded by monohydrate. *J. Phys. Chem. A* **104** (35), 8216–8223.

Churakov, S.V., 2006. Ab initio study of sorption on pyrophyllite: structure and acidity of the edge sites. *J. Phys. Chem. B* **110**, 4135–4146.

Churakov, S.V., Iannuzzi, M., Parrinello, M., 2004. Ab initio study of dehydroxylation-carbonation reaction on brucite surface. *J. Phys. Chem. B* **108** (31), 11567–11574.

CPMD, V. Copyright IBM Corp 1990–2004, Copyright MPI fuer Festkoerperforschung Stuttgart 1997–2001".

de la Pena, L.H., Kusalik, P.G., 2006. Quantum effects in liquid water and ice: model dependence. *J. Chem. Phys.* **125** (5), 054512.

Delville, A., 1991. Modeling the clay–water interface. *Langmuir* **7** (3), 547–555.

Fernandez-Serra, M.V., Artacho, E., 2004. Network equilibration and first-principles liquid water. *J. Chem. Phys.* **121** (22), 11136–11144.

Ferrage, E., Lanson, B., Malikova, N., Plancon, A., Sakharov, B.A., Drits, V.A., 2005. New insights on the distribution of interlayer water in bi-hydrated smectite from X-ray diffraction profile modeling of 001 reflections. *Chem. Mater.* **17** (13), 3499–3512.

Grim, R.E., 1968. *Clay Mineralogy*. McGraw-Hill, New York.

Grossman, J.C., Schwegler, E., Draeger, E.W., Gygi, F., Galli, G., 2004. Toward assessment of the accuracy of density functional theory for first principle simulations of water. *J. Chem. Phys.* **120**, 300–311.

Hensen, E.J.M., Smit, B., 2002. Why clays swell. *J. Phys. Chem. B* **106** (49), 12664–12667.

Hohenberg, P., Kohn, W., 1964. Inhomogeneous electron gas. *Phys. Rev.* **136** (3B), 864–871.

Iannuzzi, M., Laio, A., Parrinello, M., 2003. Efficient exploration of reactive potential energy surfaces using Car–Parrinello molecular dynamics. *Phys. Rev. Lett.* **90** (23), 238302–238306.

Kalinichev, A.G., Churakov, S.V., 2001. Thermodynamics and structure of molecular clusters in supercritical water. *Fluid Phase Equilibria* **183–184**, 271–278.

Kalinichev, A.G., Gorbaty, Y.E., Okhulkov, A.V., 1999. Structure and hydrogen bonding of liquid water at high hydrostatic pressures: Monte Carlo NPT—ensemble simulations up to 10 kbar. *J. Mol. Liquids* **82**, 57–72.

Kallay, N., Preocanin, T., Zalac, S., 2004. Standard states and activity coefficients of interfacial species. *Langmuir* **20**, 2986–2988.

Karaborni, S., Smit, B., Heidug, W., Urai, J., Oort, E.v., 1996. The swelling of clays: molecular simulations of the hydration of montmorillonit. *Science* **271** (5252), 1102–1104.

Kohn, W., Sham, L.J., 1965. Self-consistent equation including exchange and correlation effects. *Phys. Rev.* **140** (4A), A1133–A1138.

Kuo, I.-F.W., Mundy, C.J., McGrath, M.J., Siepmann, J.I., VandeVondele, J., Sprik, M., Hutter, J., Chen, B., Klein, M.L., Mohamed, F., Krack, M., Parrinello, M., 2004. Liquid water from first principles: investigation of different sampling approaches. *J. Phys. Chem. B* **108**, 12990–12998.

Kutter, S., Hansen, J.P., Sprik, M., Boek, E., 2000. Structure and phase behavior of a model clay dispersion: a molecular-dynamics investigation. *J. Chem. Phys.* **112** (1), 311–322.

Laasonen, K., Sprik, M., Parrinello, M., Car, R., 1993. "Ab initio" liquid water. *J. Chem. Phys.* **99** (11), 9080–9089.

Lee, C., Yang, W., Parr, R.G., 1988. Development of the Colle–Salvetti correlation-energy formula into a functional of the electron density. *Phys. Rev. B* **37** (2), 785–789.

Lee, J.H., Guggenheim, S., 1981. Single crystal X-Ray refinement of pyrophyllite-1Tc. *Am. Mineral.* **66**, 350–357.

Lee, S.H., Rossky, P.J., 1994. A comparison of the structure and dynamics of liquid water at hydrophobic and hydrophylic surfaces—a molecular dynamics simulations study. *J Chem. Phys.* **100**, 3334–3345.

MacKenzie, K.J.D., Brown, I.W.M., Meinhold, R.H., Bowden, M.E., 1985. Thermal reactions of pyrophyllite studied by high resolution solid state Al27 and Si29 nuclear magnetic resonance spectroscopy. *J. Am. Ceramic Soc.* **68**, 266–272.

Malikova, N., Cadene, A., Marry, V., Dubois, E., Turq, P., Zanotti, J.M., Longeville, S., 2005. Diffusion of water in clays—microscopic simulation and neutron scattering. *Chem. Phys.* **317** (2-3), 226–235.

Malikova, N., Marry, V., Dufreche, J.F., Turq, P., 2004. Na/Cs montmorillonite: temperature activation of diffusion by simulation. *Curr. Opin. Colloid Interface Sci.* **9**, 124–127.

Marx, D., Parrinello, M., 1996. Ab initio path integral molecular dynamics: basic ideas. *J. Chem. Phys.* **104** (11), 4077–4082.

Masini, P., Bernasconi, M., 2001. Ab initio simulations of hydroxylation and dehydroxylation reactions at surfaces: amorphous silica and brucite. *J. Phys. Condensed Matter* **13**, 1–12.

Molera, M., Eriksen, T., 2002. Diffusion of Na-22(+), Sr-85(2+), Cs-134(+) and Co-57(2+) in bentonite clay compacted to different densities: experiments and modeling. *Radiochimica Acta* **90** (9–11), 753–760.

Nordlund, D., Ogasawara, H., Wernet, P., Nyberg, M., Odelius, M., Pettersson, L.G.M., Nilsson, A., 2004. Surface structure of thin ice films. *Chem. Phys. Lett.* **395**, 161–165.

Odriozola, G., Aguilar, J.F., 2005. Stability of K-montmorillonite hydrates: hybrid MC simulations. *J. Chem. Theory Comput.* **1** (6), 1211–1220.

Payne, M.C., Teter, M.P., Allan, D.C., Arias, T.A., Joannopoulos, J.D., 1992. Iterative minimization techniques for ab initio total-energy calculations: molecular dynamics and conjugate gradients. *Rev. Modern Phys.* **64** (4), 1045–1097.

Perdew, J.P., Burke, K., Ernzerhof, M., 1996. Generalized gradient approximation made simple. *Phys. Rev. Lett.* **77** (18), 3865–3868.

Poinsignon, C., 1997. Proton conductivity and water dynamics in swelling clays. *Solid State Ionics* **97**, 399–407.

Schader, M.E., Yariv, S., 1990. Wettability of clay minerals. *J. Colloid Intarface Sci.* **136** (1), 85–94.

Schwegler, E., Grossman, J.C., Gygi, F., Galli, G., 2004. Towards an assessment of the accuracy of density functional theory for first principles simulations of water. II. *J. Chem. Phys.* **121**, 5400–5409.

Sit, P.H.L., Marzari, N., 2005. Static and dynamical properties of heavy water at ambient conditions from first-principles molecular dynamics. *J. Chem. Phys.* **122** (20).

Soper, A.K., 2000. The radial distribution functions of water and ice from 220 to 673 K and at pressures up to 400 MPa. *Chem. Phys.* **258** (2–3), 107–460.

Spohr, E., 1997a. Effect of electrostatic boundary conditions and system size on the interfacial properties of water and aqueous solutions. *J. Chem. Phys.* **107** (16), 6342–6348.

Spohr, E., 1997b. Molecular dynamics simulation studies of the density profiles of water between (9–3) Lennard–Jones walls. *J. Chem. Phys.* **106** (1), 388–391.

Sprik, M., Hutter, J., Parrinello, M., 1996. Ab initio molecular dynamics simulation of liquid water: comparison of three gradient-corrected density functionals. *J. Chem. Phys.* **105** (3), 1142–1152.

Sutton, R., Sposito, G., 2001. Molecular simulation of interlayer structure and dynamics in 12.4 angstrom Cs-smectite hydrates. *J. Colloid Interface Sci.* **237** (2), 174–184.

Swenson, J., Bergman, R., Howells, W.S., 2000. Quasielastic neutron scattering of two-dimensional water in a vermiculite clay. *J. Chem. Phys.* **113**, 2873–2879.

Trout, B.L., Parrinello, M., 1999. Analysis of the dissociation of H_2O in water using first-principles molecular dynamics. *J. Phys. Chem. B* **103** (34), 7340–7345.

Tunega, D., Gerzabek, M.H., Lischka, H., 2004. Ab initio molecular dynamics study of a monomolecular water layer on octahedral and tetrahedral kaolinite surfaces. *J. Phys. Chem. B* **108** (19), 5930–5936.

Tunega, D., Haberhauer, G., Gerzabek, M.H., Lischka, H., 2002. Theoretical study of adsorption sites on the (001) surfaces of 1: 1 clay minerals. *Langmuir* **18** (1), 139–147.

Van Loon, L.R., Soler, J.M., Jakob, A., Bradbury, M.H., 2003. Effect of confining pressure on the diffusion of HTO, Cl- and I- in a layered argillaceous rock (Opalinus Clay): diffusion perpendicular to the fabric. *Appl. Geochem.* **18**, 1653–1662.

Vanderbilt, D., 1990. Soft self-consistent pseudopotentials in a generalized eigenvalue formalism. *Phys. Rev. B* **41** (11), 7892–7895.

VandeVondele, J., Mohamed, F., Krack, M., Hutter, J., Sprik, M., Parrinello, M., 2005. The influence of temperature and density functional models in ab initio molecular dynamics simulation of liquid water. *J. Chem. Phys.* **122**, 014515.

Walrafen, G.E., Abebe, M., 1978. Raman studies of the bending and librational bands from water and ice VI to ~12 kbar at 32 °C. *J. Chem. Phys.* **68**, 4694–4695.

Wang, J., Kalinichev, A.G., Kirkpatrick, R.J., 2004. Molecular modeling of water structure in nano-pores between brucite (001) surfaces. *Geochim. Cosmochim. Acta* **68** (16), 3351–3365.

Warne, M.R., Allan, N.L., Cosgrove, T., 2000. Computer simulation of water molecules at kaolinite and silica surfaces. *Phys. Chem. Chem. Phys.* **2** (16), 3663–3668.

Westall, J., Hohl, H., 1980. A comparison of electrostatic models for the oxide/solution interface. *Adv. Colloid Interface Sci.* **12** (4), 265–294.

Whitley, H.D., Smith, D.E., 2004. Free energy, energy, and entropy of swelling in Cs-, Na-, and Sr-montmorillonite clays. *J. Chem. Phys.* **120** (11), 5387–5395.

Wilson, J., Cuadros, J., Cressey, G., 2004. An in situ time-resolved XRD-PSD investigation into Na–montmorillonite interlayer and particle rearrangement during dehydration. *Clay. Clay Miner.* **52** (2), 180–191.

Wilson, K.R., Cavalleri, M., Rude, B.S., Schaller, R.D., Nilsson, A., Pettersson, L.G.M., Goldman, N., Catalano, T., Bozek, J.D., Saykally, R.J., 2002. Characterization of hydrogen bond acceptor molecules at the water surface using near-edge X-ray absorption fine-structure spectroscopy and density functional theory. *J. Phys.-Condensed Matter* **14**, L221.

Yeh, I.C., Hummer, G., 2004. System-size dependence of diffusion coefficients and viscosities from molecular dynamics simulations with periodic boundary conditions. *J. Phys. Chem. B* **108** (40), 15873–15879.